NEAR-SOURCE ENERGY PARTITIONING FOR REGIONAL WAVES IN 2D AND 3D MODELS, CONTRIBUTIONS OF S*-TO-LG AND P-TO-LG SCATTERING

Xiao-Bi Xie, Thorne Lay, and Ru-Shan Wu

University of California, Santa Cruz

ABSTRACT

Regional seismic phases are now becoming of central importance for low-yield nuclear event size estimation and discrimination. However, the lack of fundamental understanding of the physics controlling regional wave energy partitioning remains a major concern for high-confidence applications of regional phases in nuclear monitoring. Due to the complex excitation and energy partitioning processes involved in regional phase formation, it is difficult to separate the contributions of different excitation mechanisms in the observed data. Given this situation, numerical simulations can play an important role for understanding the excitation of regional phases.

We develop innovative regional seismic wave numerical modeling procedures to enhance understanding of regional phase excitation and energy partitioning. Our approach is to separate the problem into consideration of near-source energy partitioning effects apart from long-range propagation effects. This is achieved by the "finite-difference modeling plus slowness analysis method". This method allows very fine 2D or 3D near source models to be used to investigate the near-source energy partitioning process. A localized slowness analysis tracks the energy partitioning instead of a time-consuming mode formation by long-distance propagator.

In this report, we focus on the frequency-dependent properties of the excitation and energy partitioning. A number of source and model parameters are calculated and examined for broad frequency ranges. As examples, *P-pS-Lg* conversion and *S*-to-Lg* excitation in the presence of near-source scattering are tested as mechanisms for *Lg*-wave excitation. The numerical results reveal that the depth of the source and the depth of the scattering process have strong effects on the *P*-to-*S* conversion and partitioning of energy into trapped or leaking signals. The *Lg*-wave excitation spectra from these mechanisms are investigated. The contributions from the scattering process are separated from those of S*-wave. The modeling shows that S*-to-*Lg* excitation is generally stronger for low frequencies and shallow source depths while *P*-to-*Lg* scattering is stronger for high frequencies. We also calculate the effect of near-source scattering on an explosion source in a 3D velocity model. The preliminary result shows that a few percent of random velocity fluctuation can generate considerable tangential waves which can be trapped in the waveguide to form the SH *L*g-wave.

OBJECTIVE

With the current emphasis on global monitoring for low-yield nuclear tests, regional seismic phases such as *Lg* have become very important for magnitude and yield estimation of underground nuclear tests. (e.g., Nuttli, 1986; Xie, et al., 1996; Patton, 2001). In addition, various *P*/*S*-type amplitude ratios for high-frequency regional phases (e.g., *Pn/Sn*, *Pn/Lg*, *Pg/Lg*, *Pg/Sn*) have become important for event discrimination (e.g., Taylor et al., 1989; Kim et al., 1993, 1997; Walter et al., 1995; Fisk et al., 1996; Taylor, 1996; Taylor and Hartse, 1997; Hartse et al., 1997; Fan and Lay, 1998a-c; Xie, 2002; Bottone et al., 2002). The applications of regional phases for yield estimation and event discrimination are largely based on empirical approaches, and while very promising in many cases, there are major questions about the nature of excitation of *S*-wave dominated phases such as *Lg*. Due to the complex excitation and energy partitioning processes associated with regional phases, it is difficult to empirically separate the contribution of individual energy partitioning mechanisms by analysis of data. Numerical modeling approaches are thus of great importance for investigating the excitation and propagation of regional phases (e.g., Wu, et al. 2000a, b; Bonner, et al., 2003; Stevens et al., 2003; Myers, et al., 2003, 2004).

Although there are continuing controversies about the dominant *P*-to-*S* transfer mechanisms affecting regional phases, most investigators agree that appreciable energy from explosion sources is converted to *S*-waves in the near-source region (e.g., Myers, et al., 2003). Several possible near-source energy excitation mechanisms have been proposed, including *P*-to-*Lg* scattering, *pS*-to-*Lg* conversion at the free surface, *Rg*-to-*Lg* coupling, *S**-to-*Lg* conversion, spall excitation of *S*, tectonic release and rock damage (e.g., Day and Mclaughlin, 1991; Gupta et al., 1992, 1997; Wallace, 1991; Gutowski, et al., 1984; Lilwall, 1988; Xie and Lay, 1994; Vogfjord, 1997; Johnson and Sammis, 2001). This project focuses on the near-source energy partitioning of regional phases in the environment prior to waveguide control on regional phase propagation. We develop the method based on 2D and 3D finite-difference simulation and local slowness analysis (FDSA method) to investigate energy partitioning right at the source region (Xie et al., 2005), while quantifying how energy will transfer into the long range propagation path, which is critical for comparisons with data. The underlying physical processes controlling the P-to-S conversion within several 10s of kilometers will be addressed. The excitation functions for different *Lg*-wave excitation mechanisms will be calculated as functions of frequency, source depth, and near-source structures

RESEARCH ACCOMPLISHED

P-*pS*-to-*Lg* and *P*-to-*Lg* Conversion

We first investigate the *P*-*pS*-to-*Lg* conversion caused by near-source lateral velocity variations and assess its effect on the explosion *S*-wave energy budget. For all numerical examples calculated in this paper, unless otherwise indicated, we use the horizontally layered Eastern Kazakh (EK) model (Priestley et al., 1988) as the background and modify it by adding random velocity fluctuations at different locations. In a horizontally layered model with overburden *P*-wave velocity larger than the upper mantle *S*-wave velocity, the free surface reflected *pS*-wave has a steep incidence angle and cannot be trapped in the crustal waveguide to form *Lg*. In this case, the energy transfer through *P*-*pS*-to-*Lg* coupling is almost zero. Although it is generally agreed that the existence of near-source lateral velocity variation can increase the *P*-to-*Lg* energy exchange, the detailed mechanism underlying this process is still not fully understood.

Figure 1 compares the simulated *P*-*pS*-to-*Lg* coupling in models with and without near surface lateral velocity variations. Figure 1a is for the EK-model. A shallow explosion source located at depth 0.5 km generates *P*, *pS* and *Rg* waves. Two-dimensional slowness analysis is conducted for selected phases in the wavefield and the results are shown together with the wavefield snapshot. The synthetic seismograms were bandpass filtered between 2.0 and 6.0 Hz before the slowness analysis. As can be seen from the result, the *P*-wave leads the wavefield and has a distinct slowness. Reverberations within the uppermost crust causes multiple parallel *pS* wavefronts with their horizontal slowness approximately equal to the overburdened *P*-slowness. The *pS* energy stays to the left of the upper-mantle *S*-slowness and there is no energy transferred from *P* to *Lg*. In Figure 1b, a shallow random velocity patch is added to the EK-model to test the effect of near surface scattering. The random patch has a 5% root mean square (RMS) velocity fluctuation (shown in the snapshot as a shaded area). The slowness analyses are conducted for *P*, *pS* and *pS*-coda. Although *P*- and early *pS*-waves are barely affected, the *pS*-coda clearly contains scattered energy with horizontal slowness to the right of the upper-mantle *S*-slowness.

Figure 2 investigates scattering taking place at deeper depths. The configuration of the source and model is similar to that used in Figure 1b, except the random patch with 3% RMS velocity fluctuation is added to the EK-model (shown in the snapshot as a shaded area). The 2D slowness analysis is conducted for selected phases in the wavefield and the results are presented in the figure. After passing through the random region, there is *P*-coda composed of scattered *P*- and *S*-waves generated from the direct *P*-wave. Although the early part of the *pS*-wave does not contribute to the trapped energy, its later part contains energy located to the right of the upper-mantle S-slowness which therefore will contribute to the trapped regional phases.
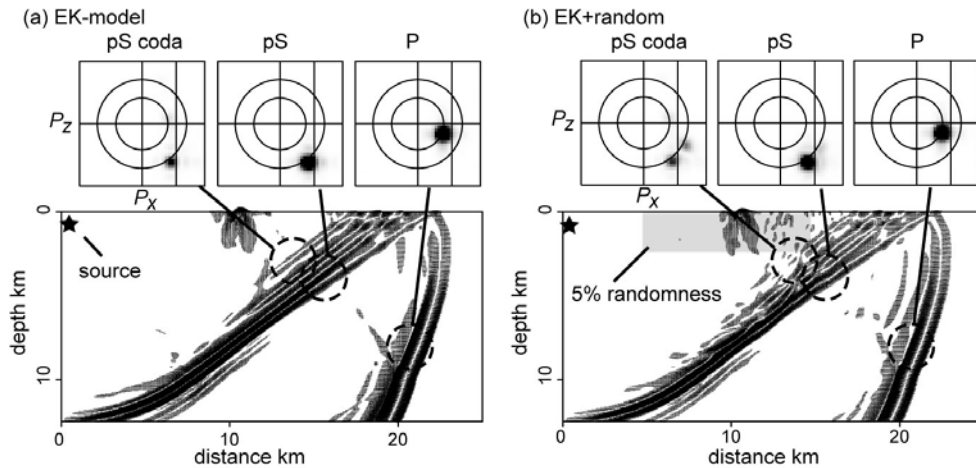
Figure 1. P-pS-to-Lg conversion due to shallow scattering. (a) is for the EK-model and (b) is for the EK-model with a shallow random patch. Details are given in the text.
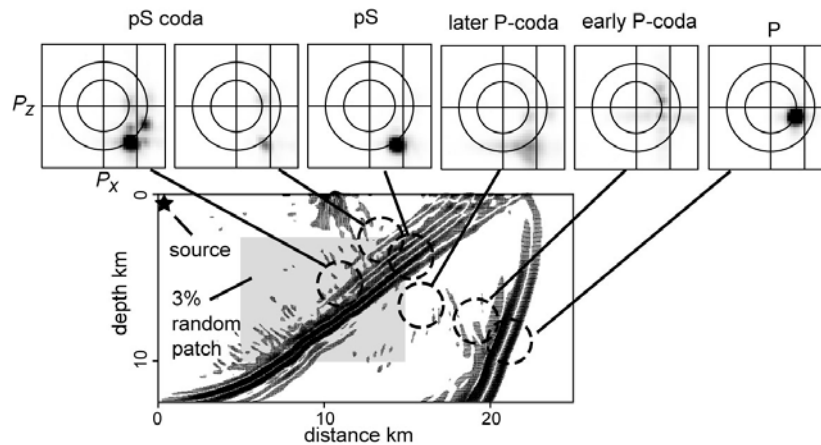
Figure 2. The P-pS-to-Lg conversion due to a deeper random patch. The slowness analysis for P, P-coda, pS and pS-coda are shown in the figure. Details are given in the text.

Figure 3 gives the energy distribution in the slowness-depth domain for different models where row (a) is for the EK-model and rows (b) and (c) are for the EK-model with 3% and 5% RMS fluctuations in a random patch like that used in Figure 2. The slowness analysis is conducted at a distance of 20 km and for depths between 0 and 12.5 km. As expected, with the EK-model no energy is seen beyond the upper mantle *S*-slowness, but after the lateral velocity variations are introduced, energy starts to build up to the right of the upper-mantle *S*-slowness. Two types of scattered energy can be found in the slowness-depth domain: weak but widely distributed *S* energy (indicated by the dashed ellipses) and scattered energy linked to the *pS*-wave (indicated by the dashed rectangles). Both types of energy satisfy the criterion $p_x \geq p_{S-mantle}$ and will contribute to the *Lg*-wave. The widely spread scattered *S*-wave is generated by the *P*-to-*Lg* coupling through volumetric scattering. The scattering process redistributes the angle spectrum of the original incident waves. Both volumetric scattering and scattering near the free-surface affect the general *P*-to-*Lg* conversion.

Contributions from the *S**-Wave

For shallow explosion sources, the *S**-wave may become a significant contributor to *Lg* (Gutowski, et al., 1984; Lilwall, 1988; Xie and Lay, 1994; Vogfjord, 1997). The amplitude of *S** can be large if the source depth is within a fraction of a wavelength from an interface. This makes its excitation highly dependent on the source depth and frequency. We investigate the contribution of the *S**-wave within the EK model. Figure 4 shows horizontal slowness analyses at a distance 35 km and for depths between 0 and 30 km. The time window is chosen between 11 to 13 s after the direct *P*-wave passes the receiver array. The synthetic seismograms are bandpass filtered between 1.0 - 5.0 Hz. The four rows from top to the bottom correspond to source depths 0.25 km, 0.5 km, 1.0 km, and 2.0 km, respectively. The major arrival is the down-going free surface reflected *pS*-wave, which has a horizontal slowness similar to the overburden *P*-slowness. As expected for a horizontally layered model, the *pS* energy stays to the left of the upper mantle *S*-slowness and has no contribution to the trapped regional phases. For shallow sources, the *Rg*-wave enters the array at about 12 s and its energy concentrates between 0 to 3 km, as can be seen on the upper right corners in the slowness-depth domain. For source depth of 2.0 km, the *Rg*-wave is very weak. The *S**-wave enters the array from a shallow depth and gradually merges with the *pS*-wave. The *S**-wave is strong for shallow sources and its amplitude decreases with increasing source depth. Very little *S** energy can be observed for source depths below 2 km. In the joint domains, the *S**-energy can be isolated and quantified even within a complicated wavefield, which is very difficult using remote surface synthetics. The dashed rectangles are the time-slowness-depth window used to locate the *S** energy. The energy from successive windows can be summed together to give the contribution of *S** to the trapped regional phases.
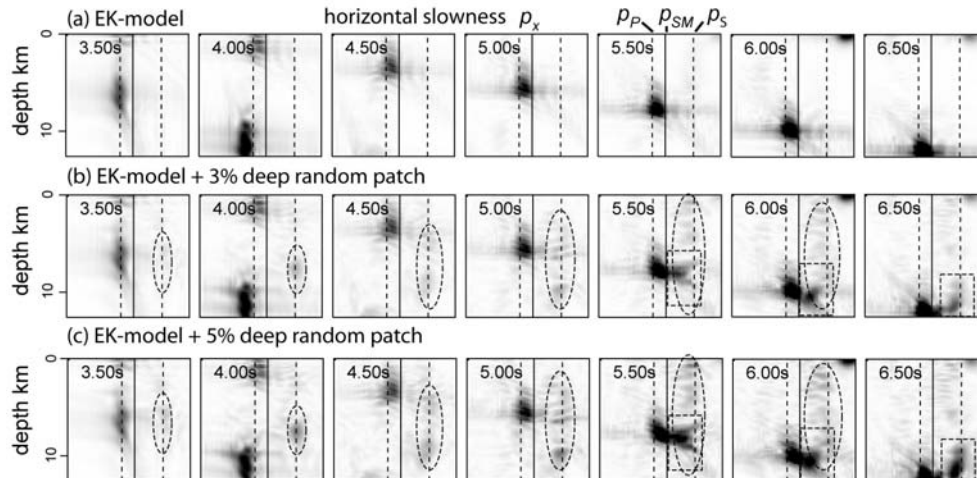
Figure 3. Energy distribution in depth and horizontal slowness domain for (a) the EK-model, (b) EK-model plus a 3% random patch and (c) EK-model plus a 5% random patch. The configuration of the source and model is same as that used in Figure 2. Energy circled by dashed rectangles is P-pS-to-Lg scattering and energy circled by dashed ellipses is P-to-Lg scattering.

The Frequency Dependent *Lg* Excitation Function

The frequency dependence of *Lg*-wave excitation is rooted in the underlying physical processes and is usually controlled by different characteristic scales. The excitation spectra from individual or joint mechanisms contributing to regional phases depict the frequency dependence of these processes. Frequency dependent *P/S* ratios will depend on the excitation functions of multiple phases. We use FDSA to quantify *Lg*-wave excitation spectra from *S**- and *pS*-waves. Figure 5 gives the *S**-to-*Lg* excitation spectra as functions of source depth and frequency. A series of bandpass filters is used to give responses at different frequencies. The vertical coordinate is the normalized relative energy $(E/E_0)^{1/2}$. Since the source spectrum has been taken away, the excitation function is the impulse response of the model to the source. The results clearly show that the *S**-to-*Lg* excitation is generally enhanced for lower frequency and shallow source depth. The major contribution comes from sources located above 1 km. For sources at depths below 1 km, only low-frequency energy below 1 Hz has significant contribution to *Lg*-wave excitation. However, the responses are also model dependent. For a model with a homogeneous crust (Figure 5a), the distribution has simple monotonic tendencies in both source depth and frequency. For the EK model (Figure 5b), the

excitation spectrum has a maximum at depth 1 km and a more complicated frequency dependence. This may reflect the fact that the EK model has an interface at 1 km depth.

To investigate the combined effect for *S**-wave and near-source scattering, we add shallow random velocity patches to the EK model. The random patch extends between distances of 5 to 25 km and depths of 0 to 2.5 km. Shown in Figures 6a and b are excitation spectra for random patches with RMS velocity fluctuations of 3% and 5%, respectively. The most prominent feature is the build up of high-frequency energy. The scattered energy increases with RMS velocity fluctuations. Figures 6c and d isolate the scattered energy by subtracting the excitation spectrum of the EK-model from the spectra for models with random velocity patches. Two types of energy can be identified within the frequency-depth domain. The high-frequency energy results from *P*-*pS*-to-*Lg* and *P*-to-*Lg* scattering. This energy is especially important for deeper sources to generate *Lg*-waves, since a deeper source generates little trapped energy in a horizontally layered model. The low-frequency energy concentrated at shallow source depths comes from *Rg*-to-*Lg* scattering.
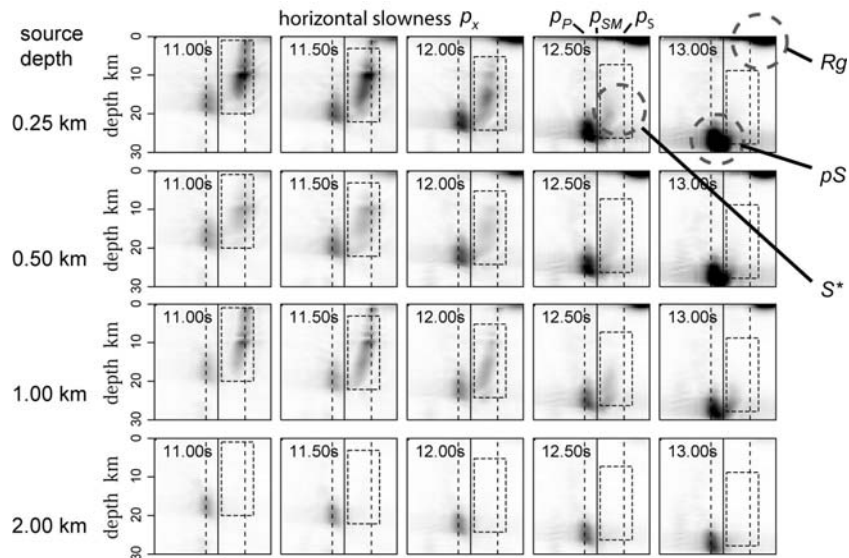
Figure 4. Slowness analysis for investigating S*-to-Lg conversion. Different rows are for different source depths. Dashed rectangles indicate the time-space-slowness windows used to pick the S* energy.
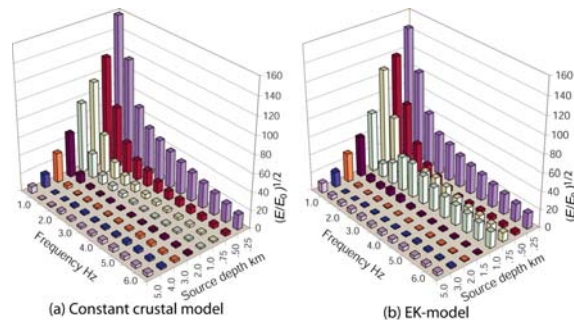
Figure 5. Normalized Lg excitation spectra for sources in different velocity models and at different depths with (a) a model with a homogeneous crust and (b) the EK-model.

Figure 7 gives the excitation spectra for the EK-model with deeper random patches. The random patch is located between distances 5 to 25 km and depths 7.5 to 10.0 km. Figures 6a and b give excitation spectra for random patches with RMS velocity fluctuations of 3% and 5%, respectively. Figures 7c and d give the isolated scattered energy. The scattered energy from the deeper random patches has little low-frequency content, which supports the interpretation that the low-frequency energy comes from the *Rg*-to-*Lg* scattering. The frequency dependent excitation spectra establish the relationship between the observations and the characteristics of sources and near-source structures. They provide the basis for evaluating the dominant mechanisms for *Lg*-wave excitation. Xie (2002) investigated the

Pn and *Lg* spectra from a group of explosions and found that the difference between these spectra requires a non-flat transfer function between the two phases. The *Lg*-wave excitation function obtained in this paper is the impulse response. Assuming that the *Pn* spectrum roughly represents the source spectrum, the excitation function obtained here approximates the *Pn* to *Lg* transfer function. Qualitatively, our excitation function explains the observations of Xie (2002) which require a non-flat *Pn* to *Lg* transfer function with an enhanced low-frequency excitation for *Lg*. To make a quantitative comparison, additional investigation is required.

(a) EK+3% shallow random   (b) EK+5% shallow random   (c) EK+3% scattered energy   (d) EK+5% scattered energy
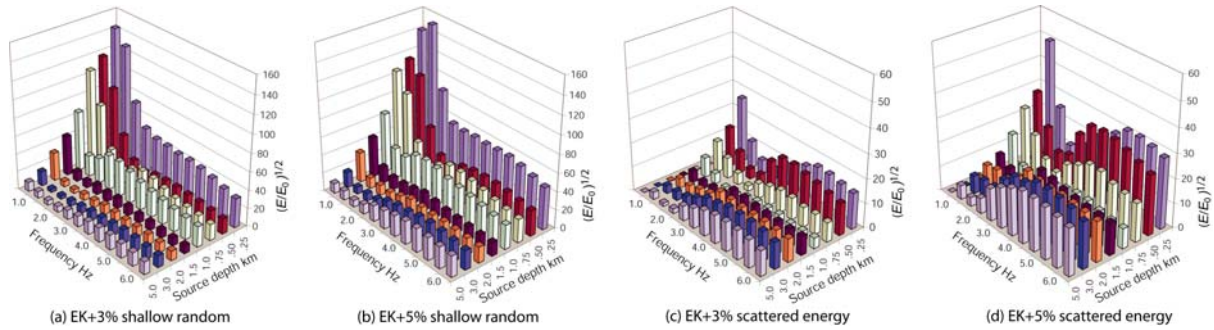
Figure 6. Normalized Lg excitation spectra for sources in the EK-model with shallow random patches, for (a) the EK-model with a 3% shallow random patch, (b) the EK-model with a 5% shallow random patch, (c) and (d) the isolated scattered energy in (a) and (b) respectively due to the random patches found by removing the energy for the layered models. Note different vertical scales are used for scattered energy.

(a) EK+3% deep random   (b) EK+5% deep random   (c) EK+3% scattered energy   (d) EK+5% scattered energy
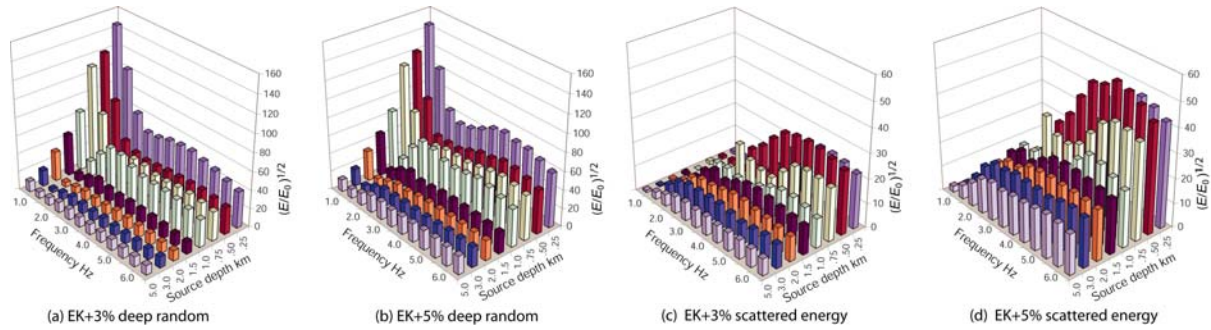
Figure 7. Normalized Lg excitation spectra for sources in the EK-model with deep random patches, for (a) the EK-model with a 3% deep random patch, (b) EK-model with a 5% deep random patch, (c) and (d) the isolated scattered energy in (a) and (b) due to the random patches.
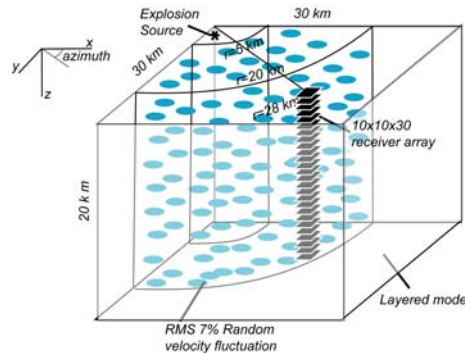
Figure 8. Cartoon showing the configuration of the 3D velocity model, source, and receiver array.

The 3D Slowness Analysis and the Excitation of SH Component

Although most Lg observations are taken from the vertical component of seismograms, the tangential component often has as much energy as the vertical component (e.g., Stevens, et al. 2003). Some researchers pointed out that at

the close range, clear SH energy comparable to that on the SV component can be observed and must be generated in the source region. Any Lg-wave excitation theory must provide an explanation for these observations. Since 2D geometry decouples the P-SV problem and the SH problem, it does not provide any information on the coupling between the source and SH component. We have conducted preliminary work to develop the 3D FDSA. A three dimensional velocity model is used to simulate the near source environment. The size of the model is 30 km $\times$ 30 km $\times$ 20 km, and the upper crust structure from the EK model is used as the background velocity. To test the effect of the heterogeneities on the P-S coupling, 7% RMS broadband random perturbation is added to P-, S-wave velocities and the density between two cylindrical surfaces around the z-axis. An eighth-order, staggered format 3D elastic finite difference code is used to generate synthetic seismograms. The grid interval used is 0.1 km. The explosion source is located at depth 0.5 km and the dominant frequency is about 3 Hz. A $10 \times 10 \times 30$ 3D receiver array is located at epicentral distance 28 km and azimuth direction 45 degrees (see Figure 8 for model configuration).
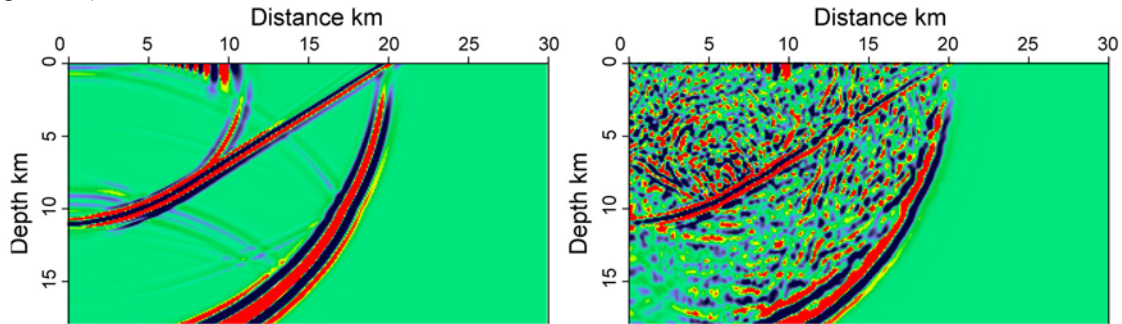
Firgure 9. Wavefield snapshot for the layered background model (left) and a laterally heterogeneous model with 7% RMS random fluctuations. Shown here is the vertical component of the displacement field.
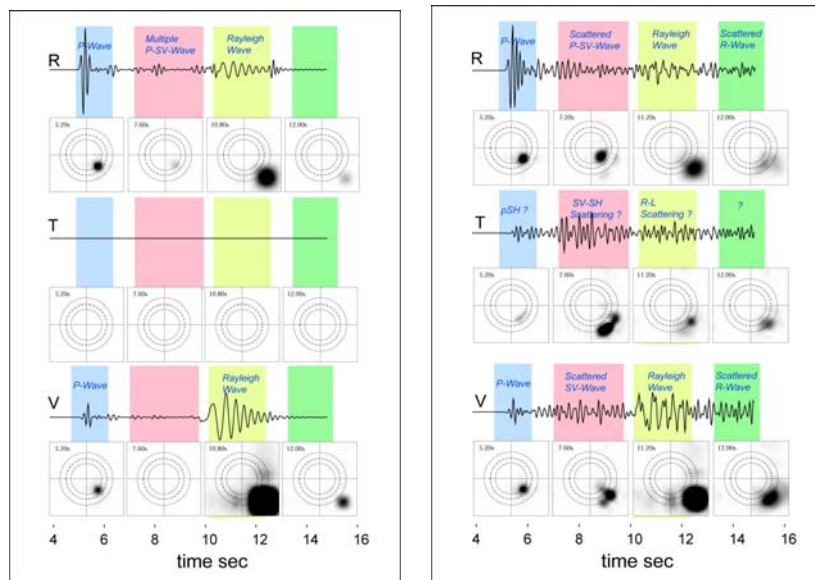
Figure 10. Comparison between synthetic seismograms and energy distribution in horizontal slowness domain for the layered velocity model (left panel) and velocity model with 7% RMS velocity fluctuations (right panel). Receivers are located at depth 1 km. All three components of the seismograms are normalized jointly but the slowness distribution for the radial component of the P-wave has been multiplied by a factor of 0.1. The P and Rayleigh waves can be clearly seen from the radial and vertical components. Note that the tangential component for the layered model is zero. For the random velocity model, scattered waves in both the tangential and vertical components can be seen. Note that much scattered energy falls outside of the upper mantle slowness (dashed line circle) and can be trapped into the crustal wave guide to form the Lg wave.

To investigate the effect of the random velocity perturbations, models both with and without the random fluctuations are calculated and their wavefield snapshots are shown in Figure 9. No surface roughness is included. Scattered energy appears in the model with random velocity fluctuations. Shown in Figures 10 are synthetic seismograms and the 2D horizontal slowness analysis from selected time windows for both the background and random models. The source depth is 0.5 km and receiver arrays are located at depth 1 km. For the background model (left panel), the P and Rayleigh waves can be clearly seen. Note the tangential component is zero. All three components of the seismograms are normalized jointly, but the slowness distribution for the radial component of the P-wave has been multiplied by a factor of 0.1. For the random model with 7% RMS velocity fluctuations (right panel), there are scattered waves in all three components including the tangential (SH) component. Much of the scattered energy falls outside of the upper mantle slowness (dashed line circle) and can thus be trapped into the crustal waveguide to form the regional phases.

Figure 11 gives the 2D horizontal slowness analysis for vertical and tangential components for the random velocity model. The receiver array is located at depth 7 km and epicentral distance 28 km. In the left panel for the vertical component, we can see that both P-wave (around 5.2 s to 5.6 s) and pS-wave (around 6.8 to 7.2 s) share the same slowness and will not contribute to the guided wave mode. Within the time window between 7.2 and 9.2 s, there is scattered P-SV energy propagating with a larger apparent horizontal slowness. The energy falls beyond the upper mantle S-wave slowness and will be trapped in the waveguide to form the P-SV Lg wave. In the right panel for the tangential component, there is considerable SH type scattered energy between 7.2 and 9.2 s with their slowness beyond the upper mantle S-wave slowness. The following features can be found from the results: (1) There is considerable SH energy excited due to the near-source lateral heterogeneities. (2) The SH energy appears to be generated through P-pS-SH or SV-SH since the SH component is relatively weak immediately following the P-wave front. The scattered energy has a broader azimuth range than the direct arrivals, which may provide a hint to reveal the actual scattering mechanisms. (3) Both SV and SH scattered energy can fall into the proper slowness region and form the crustal guided wave.
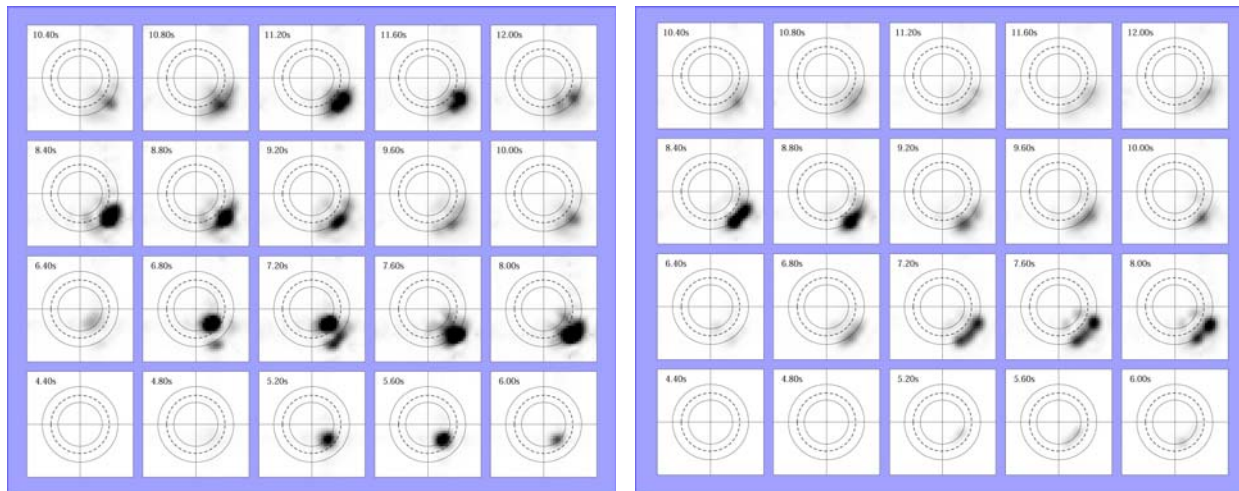
Figure 11. The wave energy distribution in the 2D horizontal slowness domain for the vertical (left) and tangential (right) components. The receiver array is located at epicentral distance 28 km and depth 7 km. Note the energy distribution outside of the upper mantle S-wave velocity.

CONCLUSIONS AND RECOMENDATIONS

A finite-difference modeling plus slowness analysis (FDSA) method has been developed to investigate near-source energy partitioning and *Lg*-wave excitation of explosive sources. The method has two major advantages. First, it allows us to study the near-source processes in multiple domains including space, time, slowness, and frequency. This provides an opportunity to isolate different mechanisms within the complex near-source environment. Second, the FDSA method can be applied at a close range, well before the *Lg*-wave is actually formed. It provides us with uncontaminated near-source information by calculating a relatively small velocity model with very fine near-source structures. Since this is a very efficient method, we can use it to investigate a broad frequency band and to test a

large number of source-model parameters. With this method, we investigated the contributions of *P-pS*-to-*Lg* conversion and *S**-to-*Lg* excitation using models with near-source random velocity fluctuations. The excitation functions of these mechanisms were also investigated. The contribution of *S**-to-*Lg* is concentrated at low frequencies and occurs for very shallow source depths. The contribution of *P-pS*-to-*Lg* coupling in the presence of near-source small-scale random heterogeneities is concentrated at high-frequencies.

The ability to handle a broad frequency band makes the FDSA an ideal tool to investigate excitation spectra and *P/S* type spectra ratios for different mechanisms and source-model parameters. The *Rg*-to-*Lg* scattering including the effect of uneven boundary topography should be included in future studies. We will further refine our 3D FDSA technique, systematically check the difference between the 2D and 3D simulations. This will help us to reevaluate the results of many previous simulations conducted on 2D models of both full-scale and near-source. It will also help us to select the problems that should be investigated using the 3D FDSA.

REFERENCES

Bonner, J. B., H. J. Patton, A. C. Rosca, H. Hooper, J. Orrey, M. Leidig, and I. Gupta (2003), Aspects of Rg and Lg generation from the Shagan depth of burial explosions, in *Proceedings of the 25th Seismic Research Review, Nuclear Explosion Monitoring: Building the Knowledge Base*, LA-UR-03-6029, 384–394.

Bottone, S., M. D. Fisk, and G. D. McCartor (2002), Regional seismic event characterization using a Bayesian formulation of simple kriging, *Bull. Seism. Soc. Am*. 92: 2277–2296.

Day, S. M. and K. L. McLaughlin (1991), Seismic source representations for spall, *Bull. Seism. Soc. Am*. 81: 191–201.

Fan, G. W. and T. Lay (1998a), Statistical analysis of irregular waveguide influences on regional seismic discriminants in China, *Bull. Seism. Soc. Am*. 88: 74–88.

Fan, G. W. and T. Lay (1998b), Regionalized versus single-station wave-guide effects on seismic discriminants in western China, *Bull. Seism. Soc. Am*. 88: 1260–1274.

Fan, G. W. and T. Lay (1998c), Statistical analysis of irregular waveguide influences on regional seismic discriminants in China: additional results for Pn/Sn, Pn/Lg and Pg/Sn, *Bull. Seism. Soc. Am*. 88: 1504–1510.

Fisk, M. D., H. L. Gray, and G. D. McCartor (1996), Regional discrimination without transporting thresholds, *Bull. Seism. Soc. Am*. 86: 1545–1558.

Gupta, I. N., W. Chan, and R. Wagner (1992). A comparison of regional phases from underground nuclear explosions at East Kazakh and Nevada Test Sites, *Bull. Seism. Soc, Am*. 82: 352–382.

Gupta, I. N., T. Zhang, and R. A. Wagner (1997), Low-frequency Lg from NTS and Kazakh nuclear explosions: observations and interpretations, *Bull. Seism. Soc. Am*. 87: 1115–1125.

Gutowski, P. R., F. Hron, D. E. Wagner, and S. Treitel (1984), S*, *Bull. Seism. Soc. Am*. 74: 61–78.

Hartse, H. E., S. R., Taylor, W. S., Phillips, and G. E. Randall, 1997, A preliminary study of regional seismic discrimination in central Asia with emphasis on western China, *Bull. Seism. Soc. Am*., 87: 551–568.

Johnson, L. R. and C. G. Sammis (2001), Effects of rock damage on seismic waves generated by explosions, *Pageoph*, 158: 1869–1908.

Kim, W. Y., V. Aharonian, A. L. Lerner-Lam, and P. G. Richards (1997), Discrimination of earthquakes and explosions in southern Russia using regional high-frequency three-component data from IRIS/JSP Caucasus Network, *Bull. Seism. Soc. Am*. 87: 569–588.

Kim, W. Y., D. W. Simpson, and P. G. Richards (1993), Discrimination of earthquakes and explosions in the eastern United States using regional high-frequency data, *Geophys. Res. Lett*. 20: 1507–1510.

Lilwall, R. C., (1988), Regional m_b:M_s, Lg/Pg amplitude ratios and Lg spectral ratios as criteria for distinguishing between earthquakes and explosions: a theoretical study, *Geophys. J. Int.*, 93: 137–147.

Myers, S. C., J. L. Wagoner, S. C. Larsen, A. Rodgers, K. Mayeda, K. D. Smith, and W. R. Walter (2003), Simulation of regional explosion S-phases (SIRES) project, in *Proceedings of the 25th Seismic Research Review, Nuclear Explosion Monitoring: Building the Knowledge Base*, LA-UR-03-6029, 117–124.

Myers, S. C., L. Preston, J. L.Wagoner, S. C. Larsen, K. D. Smith, and W. R. Walter, (2004), Simulation of regional explosion S-phases (SIRES) project, in *Proceedings of the 26th Seismic Research Review: Trends in Nuclear Explosion Monitoring*, LA-UR-04-5801, 124–133.

Nuttli, O. W. (1986), Yield estimates of Nevada Test Site explosions obtained from Lg waves, *J. Geophys. Res*. 91: 2137–2151.

Priestley, K. F., G. Zandt, and G. E. Randall (1988), Crustal structure in Eastern Kazakh, USSR from teleseismic receiver functions, *Geophys. Res. Lett*. 15: 613–616.

Patton, H. J. (2001), Regional magnitude scaling, transportability, and Ms:mb discrimination at small magnitudes, *Pageoph*, 158: 1951–2015.

Stevens, J. L., G. E. Baker, H. Xu, T. J. Bennett, N. Rimer, and S. M. Day (2003), The physical basis of Lg generation by explosion sources, in *Proceedings of the 25th Seismic Research Review, Nuclear Explosion Monitoring: Building the Knowledge Base*, LA-UR-03-6029, 456–465.

Taylor, S. R. (1996), Analysis of high frequency Pn/Lg ratios from NTS explosions and western U.S. earthquakes, *Bull. Seism. Soc. Am*. 86: 1042–1053.

Taylor, S. R., M. D. Denny, E. S. Vergino, and R.E. Glaser (1989), Regional discrimination between NTS explosions and western U.S. earthquakes, *Bull. Seism. Soc. Am*. 79: 1142–1176.

Taylor, S. R. and H. E. Hartse (1997), An evaluation of generalized likelihood ratio outlier detection to identification of seismic events in Western China, *Bull. Seism. Soc. Am*. 87: 824-831.

Vogfjord, K. S. (1997), Effects of explosion depth and earth structure on the excitation of Lg waves: S* revisited, *Bull. Seism. Soc. Am*. 87: 1100–1114.

Wallace, T. C. (1991), Body wave observations of tectonic release, in: S.R. Taylor, H.J. Patton and P.G. Richards (editors), *Explosion Source Phenomenology*, American Geophysical Union, 161–170.

Walter, W. R., K. M. Mayeda, and H. Patton (1995), Phase and spectral ratio discrimination between NTS earthquakes and explosions, Part I: Empirical observations, *Bull. Seism. Soc. Am.* 85: 1050–1067.

Wu, R. S., S. Jin and X. B. Xie (2000a), Seismic wave propagation and scattering in heterogeneous crustal waveguides using screen propagators: I SH waves, *Bull. Seism. Soc. Am*. 90: 401–413.

Wu, R. S., S. Jin and X. B. Xie (2000b), Energy partition and attenuation of Lg waves by numerical simulations using screen propagators, *Phys. Earth and Planet. Inter*. 120: 227–243.

Xie, J. (2002), Source scaling of Pn and Lg spectra and their ratios from explosions in central Asia: Implications for the identification of small seismic events at regional distances, *J. Geophys. Res*. 107: B7, 10.1029/2001JB000509.

Xie, J., L. L. Cong, characteristics of and B.J. Mitchell (1996), Spectral characteristics of the excitation and propagation of Lg from underground nuclear explosions in central Asia, *J. Geophys. Res*. 101: 5813–5822.

Xie, X. B. and T. Lay (1994), The excitation of Lg waves by explosions: A finite-difference investigation, *Bull. Seism. Soc. Am*. 84: 324–342.

Xie, X. B., Z. Ge ,and T. Lay (2005), Investigating explosion source energy partitioning and Lg-wave excitation using a finite-Difference plus slowness analysis method, submitted to *Bull. Seism. Soc. Am*.